Climate Dynamics (2002) 19: 331–342
DOI 10.1007/s00382-002-0230-3

Y. Tang

Hybrid coupled models of the tropical Pacific: I interannual variability

Received: 20 August 2001 / Accepted: 11 January 2002 / Published online: 10 April 2002

Abstract Two hybrid coupled models (HCMs), an intermediate complexity dynamical ocean model coupled to either a nonlinear neural network atmosphere (NHCM) or a linear regression atmosphere (LHCM), have been developed for the tropical Pacific. The ENSO (El Niño-Southern Oscillation) characteristics of the two coupled models were investigated. The results show that the NHCM can produce more realistic ENSO oscillatory behavior, with a period of about 57 months in comparison with a period of 87 months in the LHCM. With the gradual increase of coupling strength, both NHCM and LHCM exhibit phase-locking, eventually becoming a biennial oscillation with ENSO peaks in winter, indicating that the seasonal cycle is important in the low-frequency oscillations of both coupled models. The NHCM phase-locking is more realistically distributed among the calendar months, in the contrast to the very narrow phase-locking of the LHCM. Sensitivity experiments show that in the absence of external forcing, neither NHCM nor LHCM displays the irregular behavior of ENSO oscillations, suggesting that nonlinear chaotic behavior might not play a central role in ENSO oscillations, and stochastic forcing is likely to produce the irregularity of ENSO oscillations.

1 Introduction

The El Niño-Southern Oscillation (ENSO), a coupled atmosphere–ocean interaction centered in the tropical Pacific, has received wide attention because it has a profound influence on weather and climate on a global scale. Over the last decade, a considerable number of coupled atmosphere–ocean models have been developed to investigate its physical mechanisms and to improve its prediction. These coupled models include simple models (e.g., Suarez and Schopf 1988; Hirst 1986), intermediate coupled models (e.g., Zebiak and Cane 1987; Anderson and McCreary 1985), hybrid models (e.g., Barnett et al. 1993; Balmaseda et al. 1994,1995), and fully coupled general circulation models (GCMs) (e.g., Philander et al. 1992; Latif et al. 1993). These model studies led to better understanding of the mechanism of ENSO (Schopf and Suarez 1988; Battisti 1988; Jin et al. 1994; Tziperman et al. 1995; Chang et al. 1995), and better forecasting capability (Zebiak and Cane 1987; Barnett et al. 1993; Balmaseda et al. 1995).

One category of the coupled models, the hybrid coupled model, has been widely applied in the understanding and prediction of ENSO (Barnett et al. 1993; Davey et al. 1994; Chang et al. 1995; Syu et al. 1995; Balmaseda et al. 1994, 1995; Blanke et al. 1997; Eckert and Latif 1997). A hybrid-coupled model (HCM) usually connects a statistical atmospheric model to a dynamical ocean model. Advantages of an HCM are: (1) low computing cost compared to a GCM, (2) intermediate complexity leading to an easier understanding of the coupling mechanisms than a fully coupled GCM, and (3) avoidance of over-simplifications of nonlinear processes as in conceptual and simple models.

An important aspect affecting the HCM performance is the construction of the empirical atmospheric model for estimating the surface wind stress field from a given ocean state. All empirical atmospheric models used in HCMs have so far been linear statistical models. Hence in Tang et al. (2001), the possibility of improving the empirical atmospheric model by a nonlinear approach using neural networks (NN) was investigated and it was found that the nonlinear estimation method gives results that are in many ways similar to the linear estimate. The

Y. Tang
Department of Earth and Ocean Sciences,
University of British Columbia, Vancouver, BC, Canada

Present address: Y. Tang
CAOS, Courant Institute of Mathematical Sciences,
New York University, 251 Mercer Street,
New York, NY 10012, USA
E-mail: ytang@cims.nyu.edu

linear assumption had previously been made simply because nonlinear techniques were not available. Tang et al. (2001), to a certain extent, justified the linear assumption by showing how well the linear assumption held and what the nonlinear departures were. However, in Tang et al. (2001), the ocean model was not coupled with atmospheric model and all simulations were driven from uncoupled experiments. Anomalies developing in a nonlinear coupled system can be very different from those involved in an uncoupled forced system. It has been found that coupled ocean–atmosphere models based on similar physics can lead to opposite conclusions depending on details which have a negligible impact on forced simulations (Perigaud et al. 2000). In the present study, an extension of Tang et al. (2001), we coupled the ocean and atmosphere, examined the dynamical behavior of the HCM with a nonlinear atmosphere (henceforth the NHCM), and a linear atmosphere (LHCM), and investigated the differences between the NHCM and the LHCM in terms of ENSO simulation and prediction.

This work is Part I of this study, which focuses on ENSO simulation; while Part II (Tang and Hsieh 2002) focuses on ENSO prediction. Section 2 briefly describes the coupled models. Sections 3 and 4 discuss the dynamical behavior of both coupled models and display the differences between the NHCM and the LHCM. Conclusions and discussions are given in section 5.

2 Coupled model description

The ocean and atmosphere models used in this study are identical to those in Tang et al. (2001). The ocean model consists of a tropical Pacific model with six active layers allowing for an exchange of mass, momentum and heat at each layer interface by a parameterization of entrainment. With a resolution of $1.5° \times 1.5°$, the model extends from 30°N–30°S and 123°E–69°W. The time step for integration is 2 h. The ocean model was first used to make a control run, with forcing by the Florida State University (FSU) observed wind stress (Goldenberg and O'Brien 1981) from 1961–1990. The sea surface temperature (SST) from the control run was then used as the predictor in the statistical models to reconstruct the atmospheric wind stress (τ_x, τ_y). After removing the climatological seasonal cycle, an EOF (empirical orthogonal function) analysis was performed separately on each anomaly dataset of SST, τ_x and τ_y, to further extract the predictors and predictands. Only the first three EOF modes were used in the statistical model construction, as suggested by Latif et al. (1990) and Goswami and Shukla (1991). For the model SST, the first three EOF modes accounted for over 70% of the total variance; whereas the first three wind stress EOFs explained only 35% of the total variance, due to the presence of high frequency oscillations and noise in the wind stress although a 3-point temporal running mean has been used before performing EOF analysis. Finally linear regression (LR) and neural network (NN) models are applied to link these predictors and predictands to yield linear and nonlinear atmospheric models, respectively. More details of the ocean model and the linear and nonlinear atmospheric models are given in Tang et al. (2001).

After an atmospheric model has been constructed, coupling between the atmosphere and the ocean can be implemented. The SST anomalies from the ocean model are projected onto the first three EOF modes to extract the predictors. An atmospheric model (LR or NN) is then used to reconstruct the zonal wind stress τ_x, and a similar one for the meridional component τ_y. As common with statistical models, the variance of the predicted variables are lower than the variance in the observed variables, hence the wind-stress estimates are scaled up to their observed variance by an adjusting scale factor of 1.2, as in Barnett et al. (1993). The stress anomalies are further multiplied by a scalar parameter δ, i.e., the relative coupling parameter, to examine the impact of the coupling strength on ENSO oscillations. The reconstructed wind stress anomalies are added to the climatological wind stress field to force the ocean model. The coupling interval is 15 days.

3 Simulations from the standard coupling experiment

In the section, we present results of the standard coupling experiments. Standard coupling is defined as having the coupling coefficient δ equal to unity. Two coupled models, the dynamical ocean with either nonlinear atmosphere or linear atmosphere, are investigated. The ocean model is first forced by the climatological seasonal wind stress for 100 years, and is then coupled to the atmosphere and integrated forward for 100 years. As the two coupled models require about three years to reach equilibrium, the first three years of the coupled run will be removed in the following discussions. The seasonal cycle has been removed prior to the analyses performed in this section in order to explore the model's interannual variability.

3.1 Climatology features

The NHCM and LHCM SST climatology averaged over the integration of 97 years are both generally in good agreement with the observed climatology during 1961–1990 (Fig. 1) but they have slightly warmer equatorial Pacific, in particular in the 'warm pool' in the equatorial western Pacific in the NHCM (Fig. 1d) and the central and eastern Pacific in the LHCM (Fig. 1e). Both HCMs also captured well the pronounced seasonal cycle of SST in the eastern Pacific and the seasonal cycle of the zonal wind stress (not shown).

The main difference of the modeled SST climatology between the NHCM and LHCM is manifested in the 'warm pool' and the eastern Pacific (Fig. 1f), with the LHCM producing a warmer SST climatology in the eastern Pacific and colder SST climatology in the 'warm pool' than the NHCM SST climatology. These small differences do not necessarily imply that the differences in the coupled feedbacks between the NHCM and the LHCM are slight, as the climatological averaging can smooth out the nonlinear departures in the NHCM.

The atmospheric model only calculates the wind stress anomalies, which are added to the observed climatological wind stress to drive the ocean model. For a coupled model with an anomaly atmospheric component, the contributions from the coupled feedbacks to the ocean model climatology are generally smaller than from the uncoupled response of the ocean to the observed climatological winds. The good climatology simulation indicates that (1) the uncoupled model

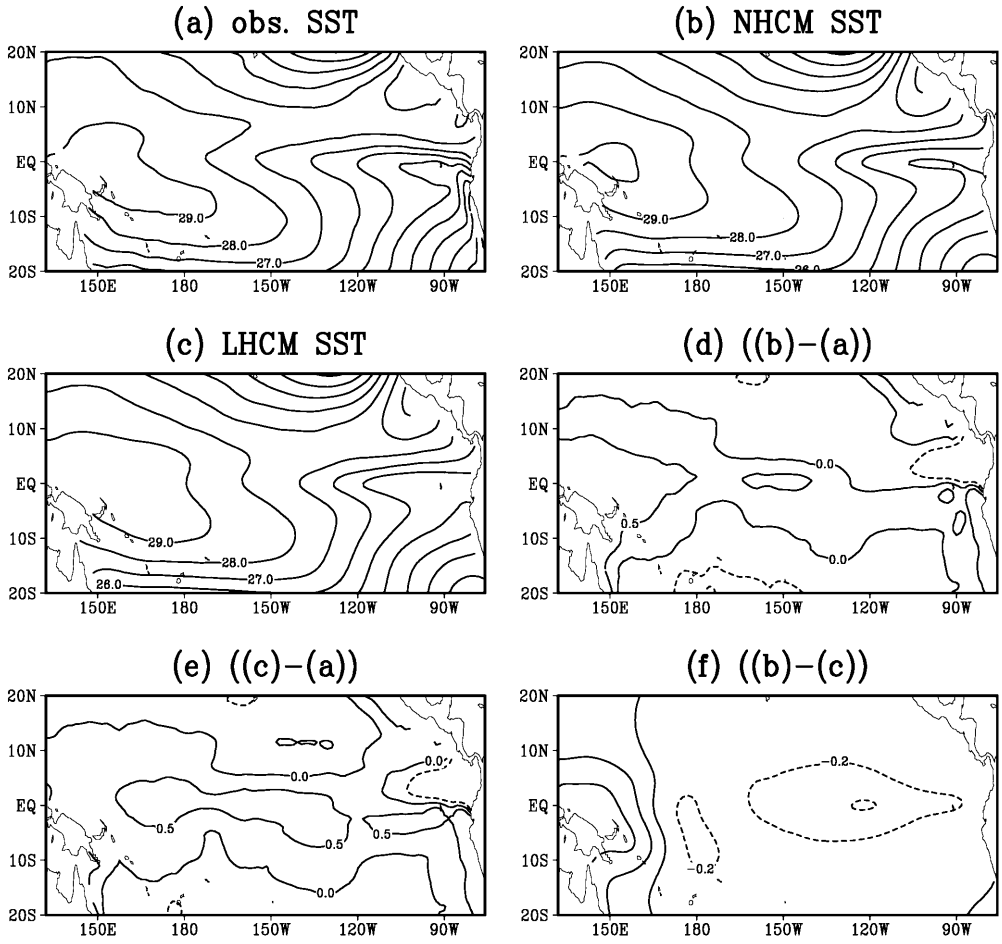

Fig. 1a–f. The SST climatology for A observations during 1961–1990, B NHCM and C LHCM, from the coupled simulations of 97 years. D Shows the difference between B and A; E, between C and D; and F, between B and C. Contour intervals are 1 °C in A–C, 0.5 °C in D–E and 0.2 °C in F. Negative contours are *dashed*

response is reasonably close to observations, and (2) the drift in the mean of the coupled system is small.

With the seasonal cycle removed, Fig. 2 compares the two leading EOF modes of the modeled SST from the NHCM with those derived from the observed SST during 1964–1990. The observed SST field is taken from the Comprehensive Ocean and Atmosphere Data Set (COADS) (Slutz et al. 1985). The first two EOFs of the modeled SST account for 53% and 24% of the total variance respectively, versus 50% and 11% of the total variance accounted for by the two leading modes from the observations. As seen in Fig. 2, the leading EOFs for the simulated SST generally resembled the observed modes, except that the simulated modes appear to be more narrowly confined to the equator, with less variability near the eastern boundary. These are common defects in all HCMs, and even in coupled GCM models (Barnett et al. 1993; Chang et al. 1996), the weak eastern boundary variability is often blamed on the poor parameterization of vertical mixing in the eastern equatorial Pacific Ocean, which will be discussed next.

The first two EOF modes of the simulated zonal wind stress and those from the observed FSU zonal wind stress (Fig. 2) reveal that the structures of simulated modes are in good agreement with those from observations. The variance accounted for by the first two modes of the NHCM modeled zonal wind stress is 81% and 10% respectively, versus 14.9% and 11.4% for the observed zonal wind stress, because of noise in the observations.

3.2 Coupling behavior

The major dynamical processes associated with the ENSO cycle in the tropical Pacific ocean are the westward off-equatorial propagation of information and the eastward propagation of information along the equator (e.g., Barnett et al. 1993; Philander 1990). To explore the main features of propagating modes in the coupled model, a principal oscillation pattern (POP) analysis has first been made for the NHCM simulations, using the 3 leading combined EOF modes of the three fields from the coupled model, SST, upper ocean heat content (HC) and zonal wind stress.

Several measures, e.g., the oscillation period T, the decay time scale and the variance contribution, as discussed in Wu et al. (1994), can be used to pick out useful or significant POP modes from the POP analysis. The ENSO-related mode is found to explain 32% of the total variance, with a period of 57 months. The spatial patterns of the POP mode are shown in Fig. 3. The POP

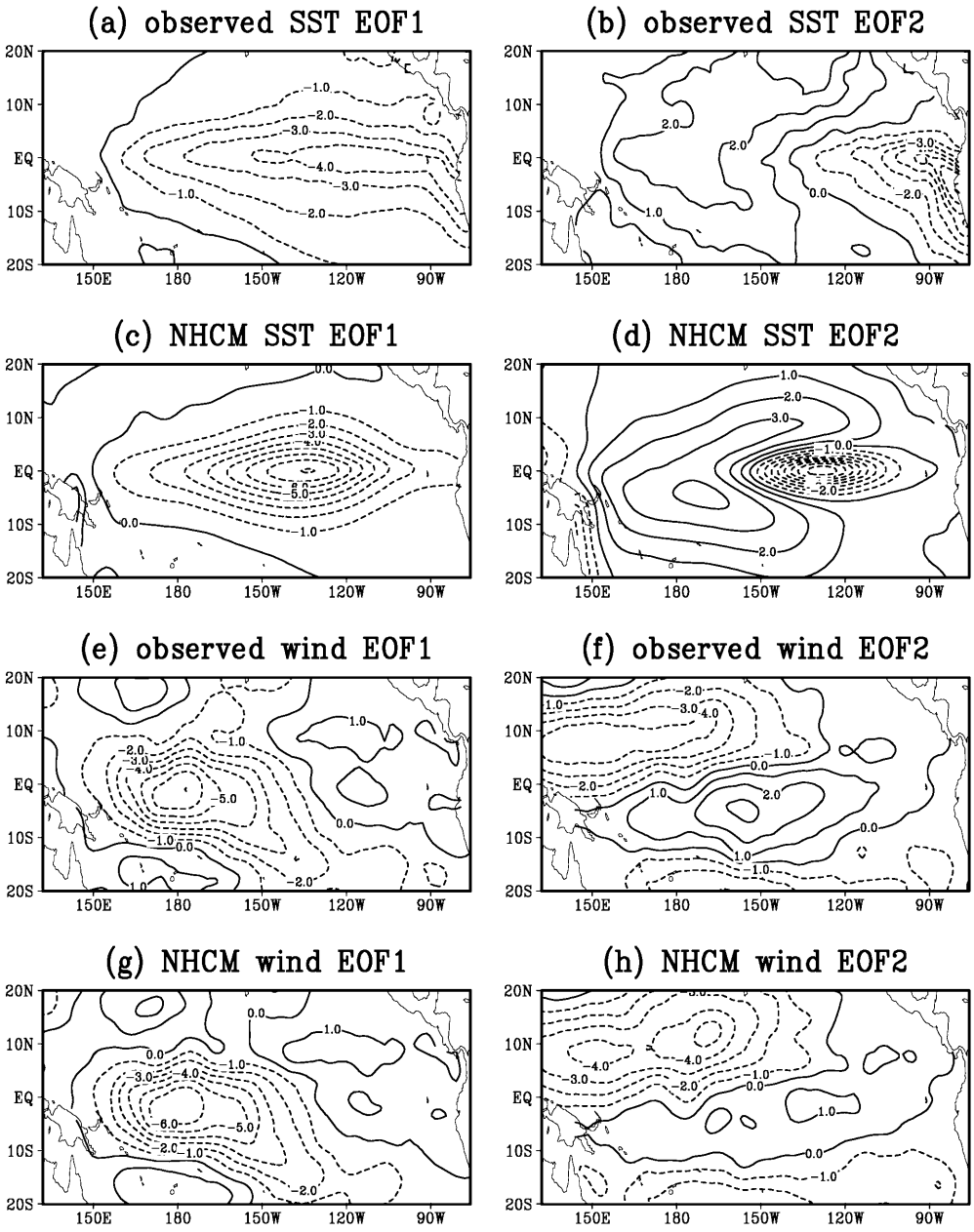

Fig. 2a–h. EOF modes 1 (*left panels*) and (2) (*right panels*) for the observed SST, the NHCM zonal wind stress, the observed zonal wind stress, and the NHCM zonal wind stress. Contour intervals = 1 °C in A–D and 1 N m^{-2} in E–H

technique interprets the pattern as evolving cyclically in time: $Q \rightarrow P \rightarrow -Q \rightarrow -P \rightarrow Q \ldots$

The characteristics of the POP patterns are very similar to those found by Balmaseda et al. (1994), Latif and Graham (1992), and Barnett et al. (1993). In the peak phase of an ENSO warm event (pattern P), the warm water present in the central equatorial and eastern Pacific Ocean yields the warm SST and HC anomalies in the region. A strong zonal HC gradient at the central equatorial Pacific weakens the upwelling there and intensifies the warm Kelvin waves propagating eastward. From the warm SST, atmospheric convection occurs, resulting in a convergence of mass and heat in the atmosphere on both sides of the equator, which enhances the oceanic upwelling in the off-equatorial regions and induces the cold westward propagating Rossby waves. The warm eastward propagating Kelvin waves bring warm waters to the eastern Pacific ocean to further intensify the anomalies; while the westward propagating Rossby waves are reflected at the western boundary as cold Kelvin waves to propagate eastward. In the theory of Weisberg and Wang (1997), a reflecting western boundary is not necessary for the ENSO oscillator. When the cold Kelvin waves arrive at the central and eastern Pacific ocean to weaken the warm anomalies in the region, the transition phase of ENSO (warm-to-cold phase) appears as the pattern $-Q$.

The zonal wind stress anomalies are closely related to the information propagation in the ocean, which can be demonstrated using Fig. 3e and Fig. 3f. During the peak phase of ENSO, large westerly wind anomalies prevail over the central equatorial Pacific associated with the

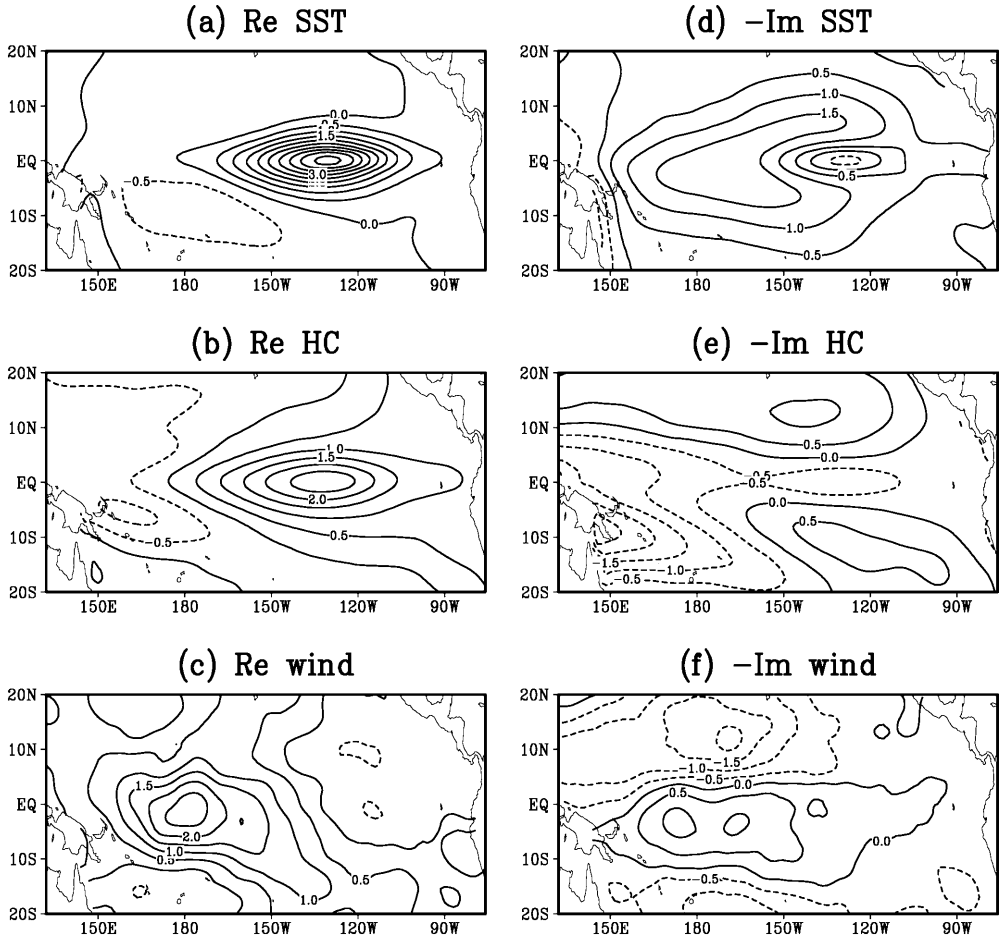

Fig. 3a–f. Spatial patterns of the ENSO-related POP mode for the NHCM. Patterns P (real) are shown on the *left*, and patterns $-Q$ (imaginary) appear on the *right*. SST anomalies are in A and D, HC anomalies are in B and E, and zonal wind stress are in C and F. Contour intervals are 0.5 °C in A,B,D and E and 0.5 N m^{-2} in C and F. The values are amplified 100 times prior to plotting

eastward propagating equatorial Kelvin wave; whereas during the transition phase ($-Q$), the westerly wind anomalies in the central equatorial Pacific are much weaker, and easterly wind anomalies dominate over much of the tropic Pacific. The wind stress anomalies in turn act on the ocean.

The POP analysis was also performed for the LHCM simulation as shown in Fig. 4, which explains 29% of the total variance. This mode has a period of 87 months, much longer than the period of the NHCM and realistic ENSO oscillations. During the peak phase, the equatorial SST anomalies change sign at 170°W (Fig. 4a), in contrast to those for the NHCM, where anomalies of the same sign reach further west, past the dateline (Fig. 3a). During the transition phase, the SST and HC anomalies are very weak in the eastern equatorial Pacific, unlike the structures found in the NHCM (Fig. 3). For the $-Q$ pattern, the easterly anomalies in the off-equatorial areas in the LHCM (Fig. 4f) are slightly weaker than the anomalies found in the NHCM (Fig. 3f). Also during this transition phase, the westerly anomalies in the central equatorial Pacific (Fig. 4f) do not withdraw as quickly as in the NHCM (Fig. 3f). The POP analysis with observed data shows that during the transition phase, the whole domain of the central equatorial Pacific is almost dominated by easterly anomalies (Latif and Flügel 1991).

The oscillatory nature of ENSO can theoretically be reproduced by equatorial processes only (e.g., Schopf and Suarez 1988; Mantua and Battisti 1994). To further explore the differences between the NHCM and the LHCM, the equatorial coupling process is examined.

Figure 5 shows the time-longitude distributions of several important variables along the equator during year 31 to year 60 in the standard coupled simulations of 100 years with the NHCM. The zonal advection of sea surface temperature is diagnosed by $-u\frac{\partial T}{\partial x}$, where T is the sea surface temperature and u the zonal velocity. Fig. 5 well depicts the typical mechanism of surface-layer feedbacks and the thermocline feedback (Neelin et al. 1998), which is associated with SSTA propagation along the equator. From the atmospheric model, alternating westerly and easterly wind anomalies lie over the central equatorial Pacific (Fig. 5c) and to the west of the SST anomalies (Fig. 5a). In the surface-layer feedback, for the warm episodes of ENSO, the surface-layer eastward current and downwelling anomalies occur under the westerlies, thus tending to reinforce the original anomaly, shifting it westward by $-u'\frac{\partial \bar{T}}{\partial x}$, the mean temperature advection by the anomalous currents in the surface-layer, contributing to the westward propagation of SSTA. The diagram for $-u\frac{\partial T}{\partial x}$ (Fig. 5b) also shows westward propagation west of 135°W. To the east of the original warm anomaly, easterly winds tend to create

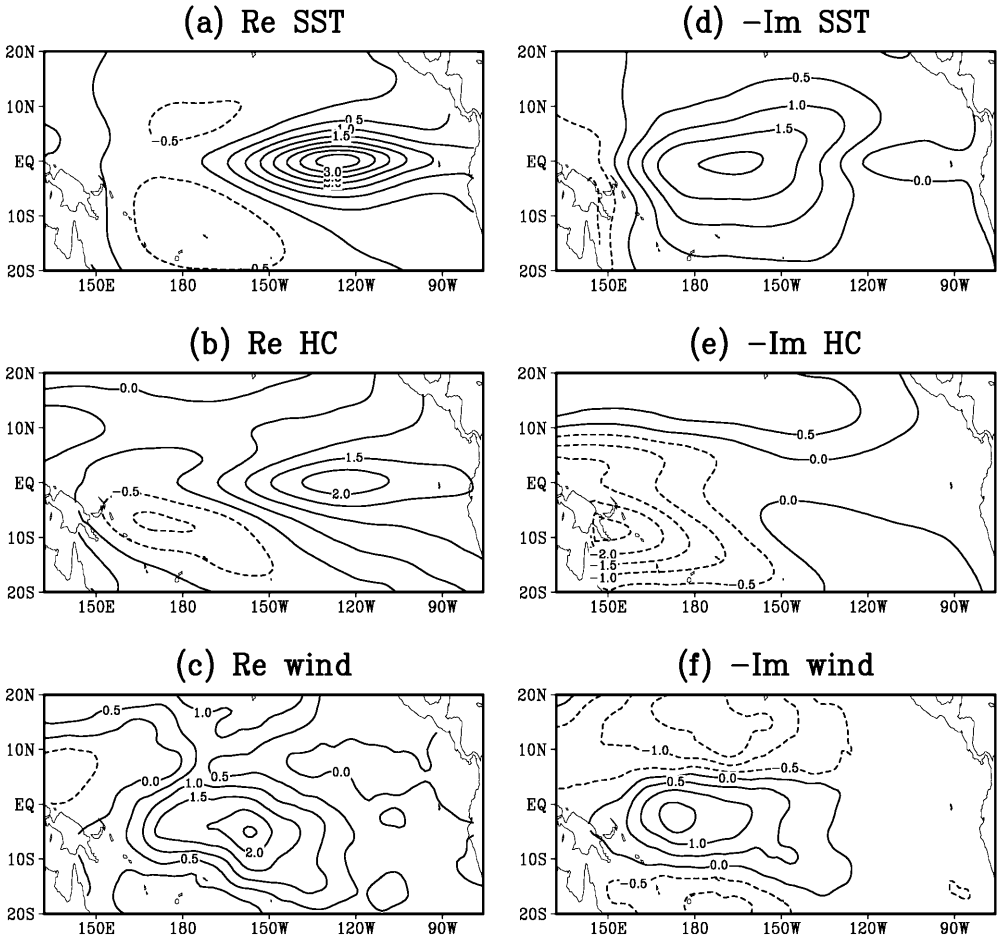

Fig. 4a–f. Same as Fig. 3 but for the LHCM simulations

cold anomalies by this mechanism, potentially resulting in a westward propagating succession of warm anomalies (Neelin et al. 1998). For the cold episodes of ENSO, analogous arguments can be applied to explain the westward propagation of the cold anomalies.

In the thermocline feedback, the westerly will shoal the thermocline in the west and deepen the thermocline in the east to balance the wind stress, creating the warm anomalies in the subsurface in the east (Fig. 5d). The warm anomalies are carried to the surface by upwelling, leading to the SSTA warm anomalies moving to the east. Likewise, the mechanism of thermocline feedback leads to the SSTA cold anomalies propagating eastward under the easterlies.

The SSTA propagation feature along the equator (Fig. 5a) can be well explained by the surface-layer feedbacks and the thermocline feedbacks, i.e., the mixed SST-ocean-dynamics modes (Neelin and Jin 1993). In the western Pacific, SSTA propagation is dominated by surface-layer feedbacks due to the deep thermocline there, whereas in the eastern Pacific, the thermocline displacements strongly affect the SSTA variations. Although the observed ENSO SST anomalies tend to appear in the cold tongue region with relatively little signature of eastward or westward propagation along the equator, almost all coupled models exhibit ENSO-like variability with noticeable propagation (Neelin et al. 1998) as in Fig. 5a. However, the propagation of SSTA anomalies in the east seems not enough strong to reach the east boundary in the NHCM, leading to rather weak SSTA variability along the coast. This is probably caused by (1) the wind anomalies triggering the thermocline displacement being not strong enough, and (2) the parameterization scheme for mixing, with a crucial role in the positive feedback between the wind and SST (Bjerknes 1969), being not very realistic in the east, in particular along the coast. Cause (1) is suggested when comparing the magnitude of the wind stress anomalies in Fig. 5 with the stronger anomalies in Fig. 6, the Hovmöller diagrams for the LHCM simulation, which will be discussed next. Cause (2) actually contributes to (1). Figure 7 is the time-longitude distributions of the change rate of SSTA from the mixing term in the eastern Pacific, diagnosed from the temperature equation (Eq. 3 in Balmaseda et al. 1994), clearly showing that the SST anomalies contributed from the mixing process is rather weak along the coast.

Figure 6 shows many features similar to Fig. 5. A major difference between them is that coupling process in the LHCM can lead to stronger anomalies for all variables than in the NHCM, associated with a longer oscillation period in the LHCM than in the NHCM, with

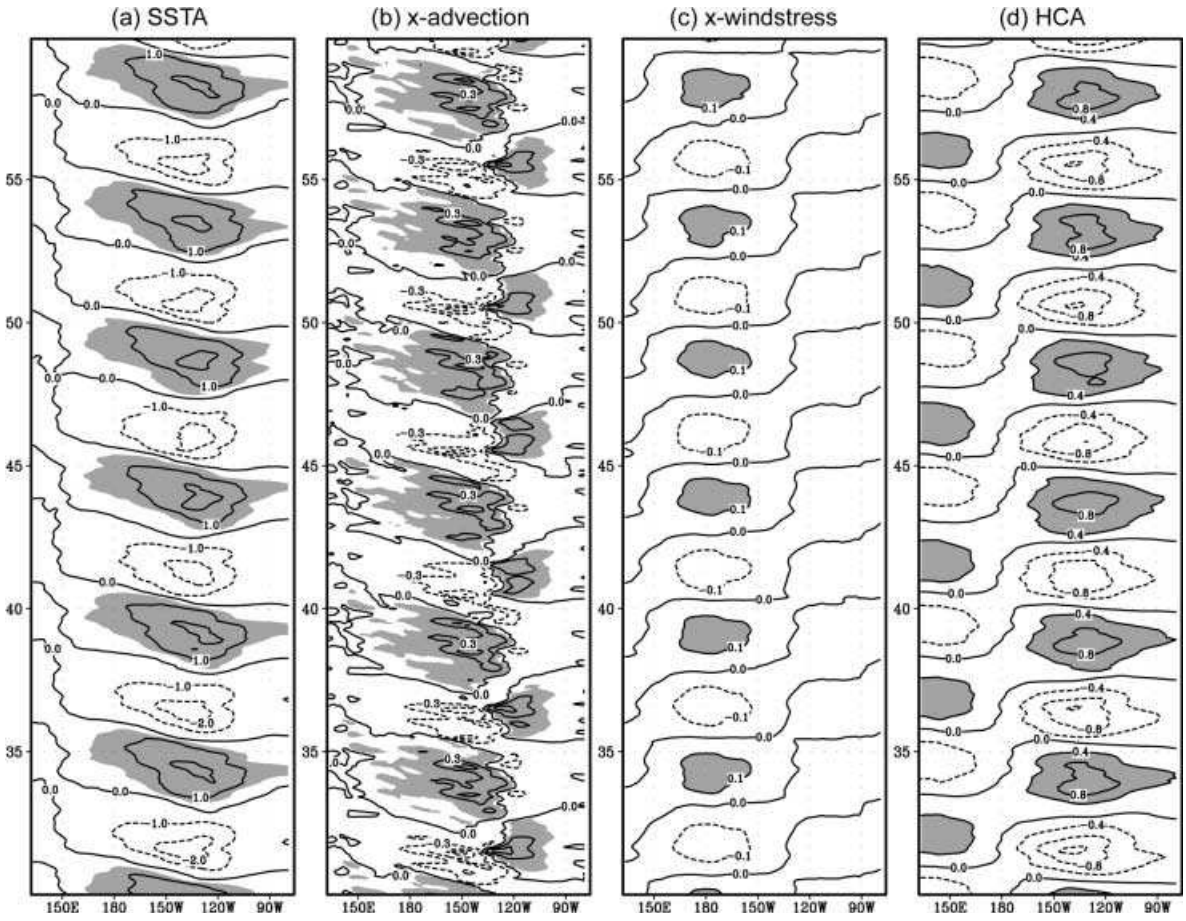

Fig. 5a–d. Time-longitude diagrams along the equator, from the coupled simulations with the NHCM, for A SSTA, B the zonal advection of sea surface temperature $-u\frac{\partial T}{\partial x}$, C the zonal wind stress anomaly, and D the heat content anomaly of the top two layers. Contour interval is 1 °C, 0.3 °C/month, 0.1 N m^{-2} and 0.4 °C in A, B, C and D respectively. The positive anomalies above 0.5 °C, 0.1 °C/month, 0.1 N m^{-2} and 0.4 °C are *shaded*. The annual cycle has been removed prior to plotting

7–8 years for the LHCM and five years for the NHCM. This is interesting because it has been found that increasing the coupling strength would shorten the oscillation period (e.g., Chang et al. 1996; Syu and Neelin 2000). The sensitivity experiments presented in next subsection also show that the period in both the NHCM and the LHCM is gradually shortened as the coupling parameter increases, suggesting that the differences of the oscillatory period between the LHCM and the NHCM performed in the standard coupling run should result from the difference of model itself, i.e., linear atmosphere versus nonlinear atmosphere, rather than from the sensitivity of the models to coupling strength. The longer period in the LHCM is well associated with the wind anomalies features in the LHCM. As shown in Fig. 6c, the westerly anomalies reside longer than the easterly anomalies, leading to more persistent warm SSTA anomalies. This is quite different with the wind anomalies in the NHCM where the westerly and easterly anomalies oscillate symmetrically, and the westerly anomalies can relatively quickly withdraw to trigger the cold SST anomalies. These features were also found in previous POP analyses (Figs. 3f and 4f).

Figure 5 and 6 also demonstrate some differences between the LHCM and the NHCM: (1) the western Pacific has a much stronger oscillation of heat content anomalies in the LHCM than in the NHCM; (2) For the LHCM, often when there is a strong anomaly of heat content in the eastern and central equatorial Pacific, there is a heat content anomaly of comparable strength but of opposite sign on the western side, which is not observed for ENSO; and (3) the westward propagation of SST anomalies is stronger and extends farther west in the LHCM than in the NHCM.

3.3 Phase-locking characteristics

An important feature of the ENSO oscillation is its phase-locking, i.e., the peaks tend to occur during a particular season. The phase-locking might be mainly due to the nonlinear interactions between the seasonal cycle and self-sustained interannual oscillations. The seasonal cycle plays a central role and often dominates the strength of phase-locking (Chang et al. 1995). Figure 8 is the histogram of the number of warm ENSO

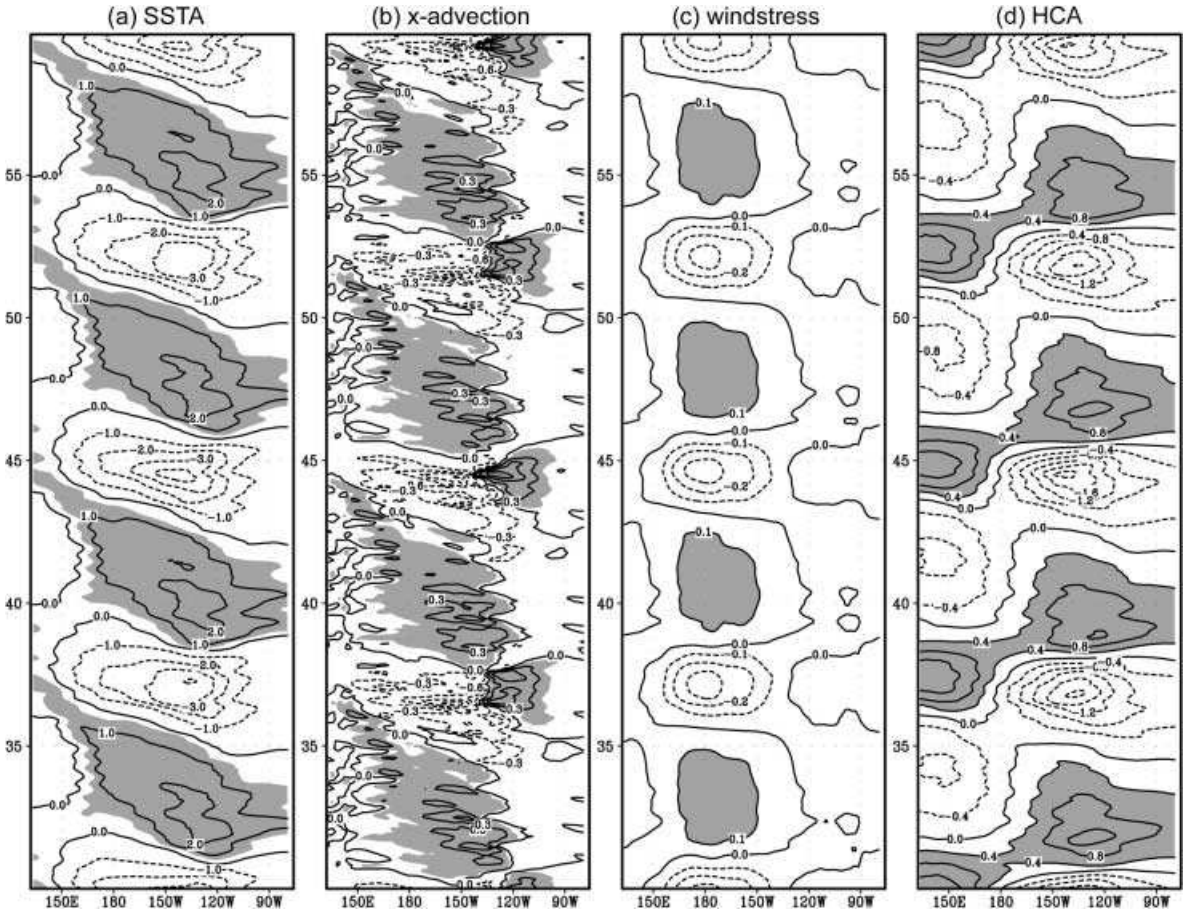

Fig. 6a–d. Same as Fig. 5 but for the LHCM simulations

events per month of the calendar year according to the time series of SST anomalies averaged over the NINO3 (150°W–90°W, 5°N–5°S) region for both coupled models. While annual phase-locking exists in both models, the phase-locking in LHCM appears to be too strong and about three months too late in comparison with observations, implying that the seasonal cycle is overemphasized in LHCM. In contrast, the more scattered phase-locking behavior and the timing of the phase-locking found in NHCM (with warm events peaking mainly in late fall and winter, and never in summer) are more realistic (Syu and Neelin 1998). The MEM (maximum entropy method) analysis of the NINO3 index derived from the NHCM simulation exhibits double significant spectral peaks at 53-month period and 28-month period, compared with only a single significant peak at 85-month period in the LHCM, revealing that the NHCM oscillations are more complicated than simply the sinusoidal oscillations found in LHCM.

4 Sensitivity experiments

To fully explore nonlinear interactions between the seasonal cycle and interannual oscillations in the two coupled models, a series of experiments were conducted by varying the coupling parameter δ. Each experiment consisted of a three-year initial spin-up followed by a 47-year simulation. The experiments show that the oscillatory behavior of both LHCM and NHCM has a sensitive dependence on the parameter, with LHCM being slightly more sensitive. In the first experiment, we decrease δ to 0.83, a value equivalent to setting the adjusting factor in Sect. 3.2 to unity for the standard coupling runs. A damped oscillation with a period of 55 months was found in the NHCM, compared with a similar oscillation with a 75-month period in the LHCM. As the coupling strength δ is gradually increased starting from the standard coupling, the oscillatory behavior of the two coupled models are basically similar to those obtained in the last section, i.e., regularity and phase-locking. As the coupling parameter increases, the period is gradually shortened. As the coupling parameter δ is further increased up to a specific critical value, the two models finally produce a two year quasi-periodic oscillation, with the peaks always occurring at the same months of the calendar year, as in many other ENSO models (Syu et al. 1995; Chang et al. 1995, 1996). The critical value is 1.5 for the LHCM and 1.68 for the NHCM. The lower critical value for the LHCM results from the LHCM being more sensitive to δ than the NHCM.

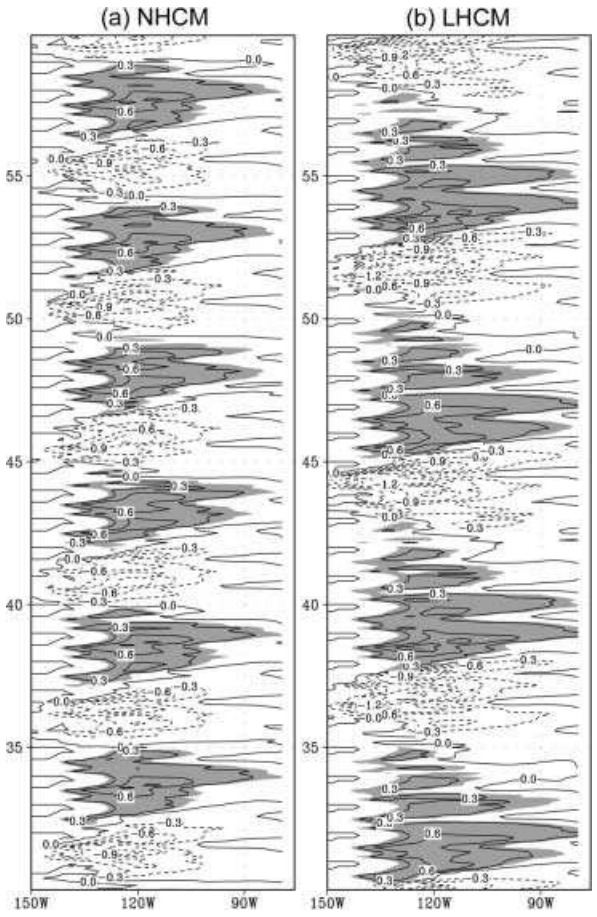

Fig. 7a, b. Time-longitude diagrams of the vertical advection term of heat (by the mixing processes, term $H(\varepsilon)$ in Eq. (3) of Balmaseda et al. 1994) for A the NHCM and B the LHCM along the equator. In the western Pacific, the values are very small and not shown. Contour interval is 0.3 °C/month, and the positive anomalies above 0.3 °C/month are *shaded*. The annual cycle has been removed prior to plotting

Frequency locking has been noted in a number of other ENSO models (Anderson and McCreary 1985; Battisti 1988; Syu et al. 1995). Chang et al. (1995, 1996) and Tziperman et al. (1995) investigated the relationship between such a frequency-locking behavior and the transition to chaos in several ENSO coupled models. They found that a further increase of the coupling strength led to chaotic behavior of the model ENSO. Interestingly, a further increase of the coupling parameter δ in our models did not exhibit the typical behavior of a chaotic system. Instead, having the coupling parameter beyond the critical value leads to a climate drift for the NHCM ($\delta = 2.0$) and for the LHCM ($\delta = 1.66$) (Fig. 9e,

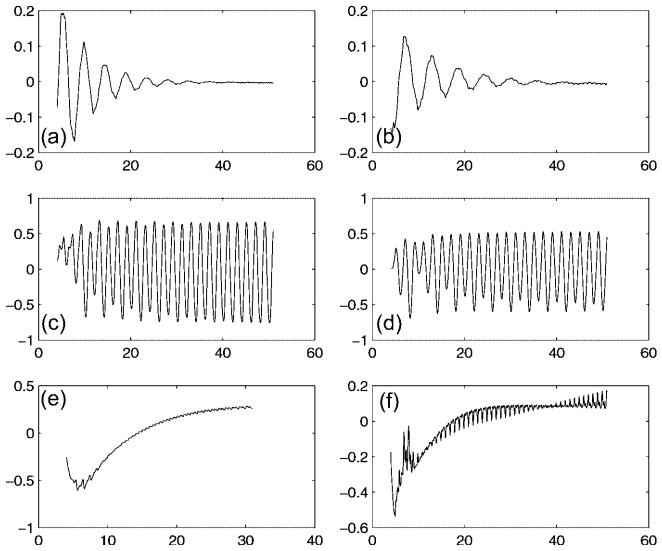

Fig. 9a–f. The time series of NINO3 index found in the NHCM and the LHCM for several cases: A, C and E for the NHCM with the coupling parameter $\delta =$ 0.83, 1.68 and 2.0 respectively; B, D and F for the LHCM with the coupling parameter $\delta =$ 0.83, 1.5 and 1.66 respectively

Fig. 8a–c. The NINO 3 index found in the NHCM and the LHCM in the standard case. The time series of NINO 3 index (*upper panel*), with *solid curve* for the NHCM and *dot-dashed curve* for the LHCM. A histogram of the number of warm events for the NHCM (*bottom-left panel*), and the LHCM (*bottom-right panel*)

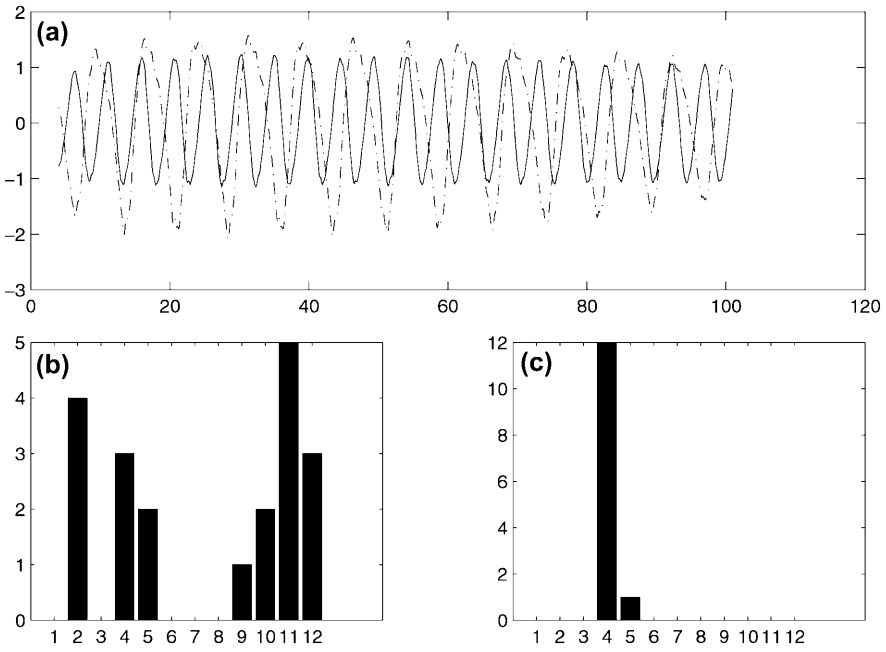

f). The climate drift at high coupling is likely associated with the spurious effects of flux correction in the coupled system as discussed in Neelin and Dijkstra (1995).

Further analyses for the NHCM and the LHCM simulations with the critical values are given in Fig. 10. A mode-locked state with a quasi-periodic cycle of two years can be found for both the NHCM and the LHCM in Fig. 10. The LHCM has a very strong phase-locking to January; but the NHCM shows a more realistic broader phase locking. In the MEM analyses, the single sharp peak at period of two years is clearly shown, and a broad spectrum, a necessary indicator of chaos, does not appear for either model. In the construction of the phase plane, we still used the methods commonly used in ENSO studies, i.e., decorrelated time step K for the time lag, and two dimensions SST(t) and SST($t + K$) for dynamical dimensions, to be consistent with the discussions of other ENSO models. Figure 10e, f shows the phase planes reconstructed with $K = 14$ months, which also clearly shows the limit cycle solution for the both models.

As we have not covered the entire parameter regime in our search, there might exist some specific parameters which can produce chaotic behavior associated with ENSO in our models, but recent works do show that the random forcing may play a central role in ENSO evolution (Blanke et al. 1997; Eckert and Latif 1997). The irregular interannual oscillation simulated by coupled CGCMs (Philander et al. 1992) does not appear to be low-order chaos. The nonlinear time series analysis performed by Chang et al. (1996) suggests that stochastic processes, rather than chaotic dynamics, are

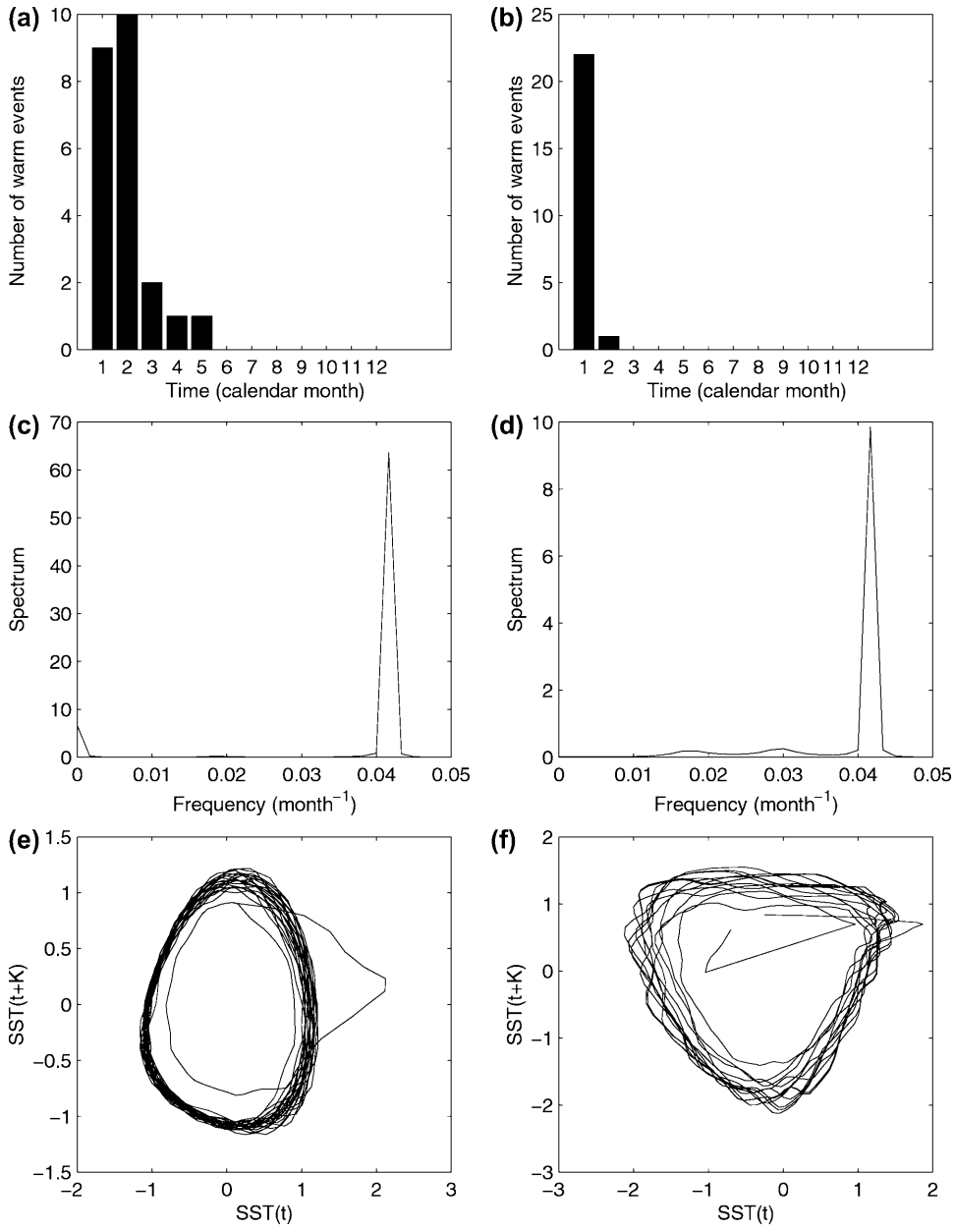

Fig. 10a–f. Analyses of the NINO3 index for the NHCM and the LHCM at the critical coupling parameter δ. The NHCM are shown on the *left* ($\delta = 1.68$), and the LHCM appear on the *right* ($\delta = 1.5$). Thus A and B are the histograms of the number of warm events for months 1 to 12 (i.e., January to December); C and D are the power spectra; E and F are the phase planes reconstructed from the time series

likely to be a major source of ENSO irregularity in CGCMs and in nature.

5 Summary and discussions

In the hierarchy of ENSO models, the linearity assumption has previously been made for the atmospheric component in hybrid couple models and many intermediate coupled models. Although this assumption has been successful in ENSO models, it is of interest to examine this assumption and explore the impact of nonlinearity of the atmosphere model on coupled simulations. In this study, we have examined the performance of the NHCM, and compared the NHCM with the LHCM, where the nonlinear neural network atmosphere is replaced by a linear regression atmosphere. Both HCMs can simulate a realistic climatology and the seasonal cycle. The major features of ENSO variability in the tropic Pacific can also be well captured. The oscillatory behavior of ENSO in both HCMs can be understood as mixed SST-ocean-dynamics modes and described by the surface-layer feedbacks and thermocline feedbacks associated with nonlinear dynamics.

The comparisons between the NHCM and the LHCM are performed based on two standard coupling runs. The major differences between the NHCM and the LHCM are: (1) the LHCM produces stronger trade wind anomalies, leading to stronger SSTA and heat content anomalies than the NHCM; (2) the westerly anomalies persist longer time than the easterly anomalies in the LHCM, resulting in the warm SSTA in the LHCM lasting much longer than the cold anomalies, whereas the NHCM produces almost symmetrical oscillation between the westerly and the easterly anomalies; (3) the NHCM can have a more realistic oscillatory period of about 4–5 years whereas the LHCM has a period of 7–8 years; and (4) the NHCM has more realistic phase-locking to the annual cycle in the distribution of the peaks of its ENSO warm events.

Model sensitivity studies demonstrated that both the NHCM and the LHCM are sensitive to the coupling strength of the system, with the LHCM being more sensitive. Depending on the changes of the coupling parameter, both coupled models can change from a stable state (damped oscillations) to an unstable state (periodic oscillations). With the increase of the coupling strength, the seasonal cycle has more effect on the inherent oscillation of the coupled models. As the coupling parameter reaches the critical values, both models are finally locked in a biennial frequency with warm events peaking in winter.

Chaos has been suggested in many ENSO models. Our sensitivity studies do not exhibit chaotic behavior for both coupled models. Instead, for either of the coupled models, as the coupling parameter increases beyond the critical value, the model climate will shift. Hence, chaotic behavior may not play a central role for ENSO oscillations, and stochastic forcing may be the source of ENSO irregularity.

Acknowledgements I am grateful to Prof. William Hsieh for detailed comments on the original manuscript. I would like to thank two anonymous reviewers and Prof. David Neelin for their valuable comments which greatly improved the original manuscript. The ocean model was made available through the courtesy of Prof. K. Haines, Prof. D.L.T Anderson and Dr. M.A. Balmaseda. This work was supported by research and strategic grants to W. Hsieh from the Natural Sciences and Engineering Research Council of Canada.

References

Anderson DLT, McCreary JP (1985) Slowly propagating disturbances in a coupled ocean–atmosphere model. J Atmos Sci 42: 615–629

Balmaseda MA, Anderson DLT, Davey MK (1994) ENSO prediction using a dynamical ocean model coupled to statistical atmospheres, Tellus 46(A) 4: 497–511

Balmaseda MA, Davey MK, Anderson DLT (1995) Decadal and seasonal Dependence of ENSO prediction skill. J Clim 8: 2705–2715

Barnett TP, Latif M, Graham NE, Flügel M, Pazan S, White W (1993) ENSO and ENSO related predictability. Part1: Prediction of equatorial sea surface temperature with a hybrid coupled ocean–atmosphere model. J Clim 6: 1545–1566

Battisti DS (1988) Dynamics and thermodynamics of a warming event in a coupled tropical atmosphere–ocean model. J Atmos Sci 45: 2889–2919

Bjerknes J (1969) Atmospheric teleconnections from the equatorial Pacific. Mon Weather Rev 97: 163–172

Blanke B, Neelin JD, Gutzler D (1997) Estimating the effect of stochastic wind stress forcing on ENSO irregularity. J Clim 10: 1473–1486

Chang P, Ji L, Wang B, Li T (1995) Interaction between the seasonal cycle and El Niño-Southern Oscillation in an intermediate coupled ocean–atmosphere model. J Atmos Sci 52: 2353–2372

Chang P, Ji L, Li H, Flügel M (1996) Chaotic dynamics versus stochastic processes in El Niño-Southern Oscillation in coupled ocean–atmosphere models. Physica D 98: 301–320

Davey MK, Ineson S, Balmaseda MA (1994) Simulation and hindcasts of tropical Pacific Ocean interannual variability. Tellus 46A: 433–447

Eckert C, Latif M (1997) Predictability of a stochastic forced hybrid coupled model of El Niño. J Clim 10: 1488–1504

Goldenberg B, O'Brien JJ (1981) Time and space variability of tropical Pacific wind stress. Mon Weather Rev 109: 1190–1207

Goswami BN, Shukla J (1991) Predictability of a coupled ocean–atmosphere model. J Clim 4: 3–22

Hirst AC (1986) Unstable and damped equatorial models in simple coupled ocean -atmosphere models. J Clim 3: 1254–1281

Jin F-F, Neelin JD, Gill M (1994) ENSO on the devil staircase. Science 264: 70–72

Latif M, Flügel M (1991) An Investigation of short-range climate predictability in the Tropical Pacific. J Geophys Res 96: 2661–2673

Latif M, Graham NE (1992) How much predictive skills is contained in the thermal structure of an Oceanic GCM? J Phys Oceanogr 22: 951–962

Latif M, Biercamp J, von Storch H, McPhaden MJ, Kirk E (1990) Simulation of ENSO-related surface wind anomalies with an atmospheric GCM forced by observed SST. J Clim 3: 509–521

Latif M, Sterl A, Maier-Reimer E, Junge MM (1993) Climate variability in a coupled GCM. PartI) the tropical Pacific. J Clim 6: 5–21

Mantua NJ, Battisti DS (1994) Evidence for the delayed-oscillator mechanism for ENSO: the "observed" oceanic Kelvin mode in the Far Western Pacific. J Phys Oceanogr 24: 691–699

Neelin JD, Jin F-F (1993) Modes of interannual tropical ocean–atmosphere interaction – a unified view. Part II: analytical results in the weak coupling limit. J Atmos Sci 50: 3504–3522

Neelin JD, Dijkstra HA (1995) ocean–atmosphere interaction and the tropical climatology. Part I: the dangers of flux correction. Clim Dyn 12: 101–112

Neelin JD, Battisti DS, Hirst AC, Jin F-F, Wakata Y, Yamagata T, Zebiak S (1998) ENSO theory. J Geophys Res 103: 14261–14287

Perigaud C, Melin F, Cassou C (2000) ENSO simulated by intermediate coupled models and evaluated with observations over 1970–98. Part I: role of the off-equatorial variability. J Clim 13: 1605–1634

Philander SGH (1990) El Niño, La Niña, and the Southern Oscillation. Academic Press, pp 293

Philander SGH, Pacanowski RC, Lau NC, Nath MJ (1992) Simulation of ENSO with a global atmospheric GCM. J Clim 5: 308–329

Schopf PS, Suarez MJ (1988) Vacillations in a coupled ocean–atmosphere model. J Atmos Sci 45: 549–566

Slutz R, Coauthors (1985) The Comprehensive ocean–atmosphere data set release.I Climate Research Program, ERL/NOAA, Boulder, CO, pp 39

Suarez MJ, Schopf PS (1988) A delayed action oscillator for ENSO. J Atmos Sci 45: 3283–3287

Syu H-H, Neelin JD (1998) Simulation and prediction of El Niño and the variation of ENSO phase locking, Ninth Conference on Interaction of the sea and atmosphere, Phoenix, 11-16 January 1998, pp 115–119

Syu H-H, Neelin JD (2000) ENSO in a hybrid coupled model. Part I: Sensitivity to physical parameterizations. Clim Dyn 16: 19–34

Syu H-H, Neelin JD, Gutzler D (1995) Seasonal and interannual variability in a hybrid coupled GCM. J Climate 9: 2121–2143

Tang Y, Hsieh WW, Tang B, Haines K (2001) A neural network atmospheric model for hybrid coupled modeling. Clim Dyn 17: 445–455

Tang Y, Hsieh WW (2002) Hybrid coupled models of the tropical Pacific – Part II. ENSO prediction. Clim Dyn (this issue)

Tziperman E, Cane MA, Zebiak SE (1995) Irregularity and locking to the seasonal cycle in an ENSO prediction model as explained by the quasi-periodicity route to chaos. J Atmos Sci 52: 293–306

Weisberg RH, Wang C (1997) A western Pacific oscillator paradigm for the El Niño-Southern Oscillation. Geophys Res Lett 24: 779–782

Wu D-H, Anderson DLT, Davey MK (1994) ENSO prediction experiments using a simple ocean–atmosphere model. Tellus 49A: 464–480

Zebiak SE, Cane MA (1987) A model El Niño-Southern Oscillation. Mon Weather Rev 115: 2262–2278